Mathematical modeling on a novel manufacturing method for roller-gear cams using a whirl-machining process

Moeso Andrianto

Yu-Ren Wu (yurenwu@ncu.edu.tw)

National Central University https://orcid.org/0000-0001-5856-2944

Achmad Arifin

Research Article

Keywords: whirl-machining, roller-gear cam, normal deviations, virtual cutting

Posted Date: October 10th, 2022

DOI: https://doi.org/10.21203/rs.3.rs-2128777/v1

Mathematical modeling on a novel manufacturing method for roller-gear cams using a whirl-machining process

Moeso Andrianto[a,b], Yu-Ren Wu[a,*], Achmad Arifin[c]

[a]Department of Mechanical Engineering, National Central University, 300 Zhongda Rd., Zhongli District, Taoyuan City 320317, Taiwan, ROC
[b]Research Center for Appropriate Technology, National Research and Innovation Agency (BRIN), Subang 41213, Indonesia
[c]Department of Mechanical Engineering Education, Universitas Negeri Yogyakarta, 01, Colombo Rd, Karangmalang, Yogyakarta 55281, Indonesia

[*]Corresponding author (Email: yurenwu@ncu.edu.tw; Tel.: 886-3-4227151 ext. 34332; Fax: 886-3-4224501)

Abstract

The whirl-machining process is a precise, efficient, and promising machine process for manufacturing workpieces over the milling process. At the same time, the roller-gear cam has advantages over the other cam-follower system. However, the whirl-machining process has not been applied to manufacture the roller-gear cam. Therefore, this paper proposes a novel method for roller-gear cam manufacturing using a whirl-machining process. Mathematical modeling is described for generating the roller-gear cam, roller, and whirl-milling tool surface. A novel CNC machine and its coordinate system are proposed. Cutting simulations for obtaining the surface topologies and normal deviations are conducted. Globoidal cam with different cylindrical rollers, globoidal cam with a conical roller, and cylindrical cam with a conical roller are taken as case studies, and results are discussed. A virtual cutting simulation was conducted using VERICUT. Some machining examples are shown to verify the benefits of the proposed method in roller-gear cam manufacturing.

Keywords: whirl-machining; roller-gear cam; normal deviations; virtual cutting.

1. Introduction

The whirl-machining process, developed by Burgsmuller (a German company) [1], has several advantages and benefits over the milling process; such as there is no need for coolant (dry machining), less cutting force, final grinding can be eliminated, and nine-times higher production rate [1-4]. Compared to milling, whirl-machining has a larger cutting area or tool contact path. A comparison of milling and whirl-machining processes can be seen in **Fig. 1**. The whirl-machining tool is an internal machining tool in which the cutter inserts are radially mounted on the inside of a whirl-machining ring. The lead angle determines the angle of inclination between the tool with the workpiece axis, and the depth of cut is determined by the eccentricity of the workpiece with the whirling ring [5]. A whirl-machining tool removes material from the workpiece and feeds it along the axis to produce a helical form [2]. The whirl-machining tools have been used in various mechanical industries, including aviation, automobiles, machine tools, motion control, implant parts, and medical components [1, 5-6]. They have primarily been used to produce cylindrical worms [4], ball screws [1, 7, 8], lead screws [9, 10], and micro screws [11]. On the other hand, whirl-machining tools have not yet been developed and studied for manufacturing roller-gear cams.

As an intermittent-motion mechanism consisting of a globoidal cam and a turret with rollers, the Roller-Gear Cam (RGC) is considered when positioning precision is required for a speed reducer [12-14]. A roller-gear cam drive consists of a roller-gear cam and several rollers, as shown in **Fig. 2**. The rollers are either cylindrical or conical. RGC is widely utilized in many machines and automation-manufacturing devices due to its advantages, such as higher load capacity, lower noise, lower vibration, higher reliability, less space, more accurate, and more compact structure compared to other cam-follower systems and intermittent-motion mechanisms [12, 15-18].

Globoidal cam geometry is an essential and significant concern in designing and manufacturing an RGC, as it is one of the most complicated cams [12, 13, 16, 17]. Litvin and Fuentes [19] proposed the method for generating the globoidal shape surface. Yan and Chen [16, 20] utilized cylindrical and hyperboloid rollers to investigate the geometry design and machining of RGC. Van and Pokorny [17] utilized a cylindrical roller and indexing turret follower for modeling concave globoidal cam. A systematic and complete method for analyzing and simulating the globoidal cam mechanism was presented by Zhang et al. [21]. RGC contact bearing has been established by Lo et al. [18]. Zongyu et al. [22], by considering the clearance, described the dynamics of the RGC system. However, they have not proposed a mathematical modeling method for manufacturing the globoidal cam using the whirl-machining process. Our purpose here is to establish novel mathematical modeling for proposing the tool for manufacturing the globoidal cam. Mathematical modeling methods of tools have been

studied in the extant literature, such as milling tool [23-26], turning tool [27], skiving tool [28], worm-shaped tool [29], barrel-shaped tool [30], form-cutting tool [31] and others [32-36]. A mathematical modeling method of the whirl-machining tool has recently been utilized to simulate double enveloping worms manufacturing [37].

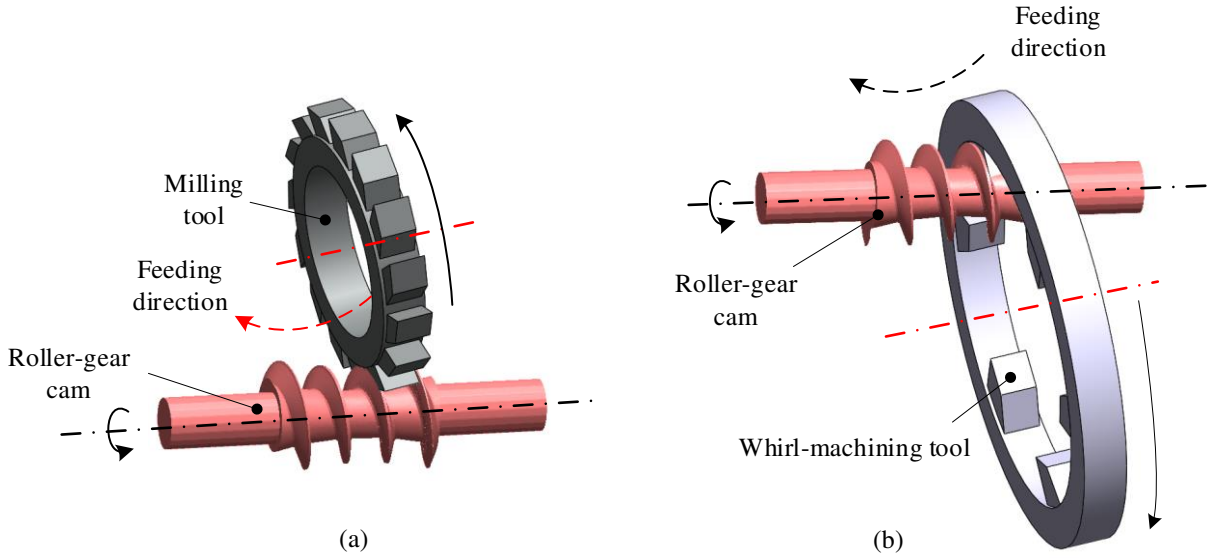

Fig. 1 Comparison of the manufacturing process: (a) Milling; (b) Whirl-machining

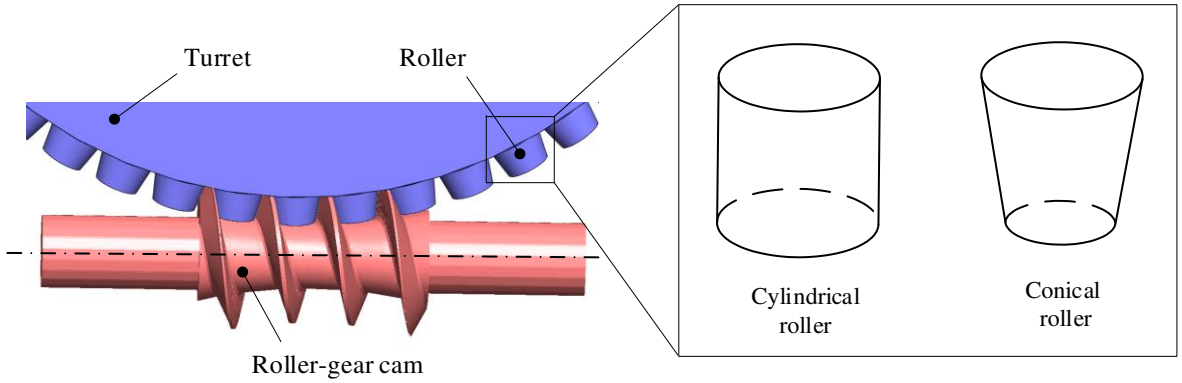

Fig. 2 Roller-gear cam drive

This paper proposes the technique of manufacturing globoidal cams with a whirl-machining tool. A workpiece with a globoidal shape is suitable with the whirl-machining method. The mathematical modeling is conducted based on the theory of gearing. A general mathematical model is investigated for generating the globoidal cam and the roller surfaces. The tool profile is generated based on the lead angle of the roller-gear cam. Cutting simulation of the whirl-machining process based on a CNC machine is conducted.

Furthermore, the contact lines on the roller-gear cam surface and the tool are achieved. Normal deviations are calculated based on comparing the technical and generated profile of the roller-gear cam. The proposed method can also be utilized for manufacturing RGC of globoidal cam with different cylindrical rollers, globoidal cam with conical rollers, and cylindrical cam with conical rollers. Numerical examples are considered for determining the accuracy and the practicability of the proposed method. A virtual cutting simulation was conducted.

2. Mathematical model for generating the whirl-machining tool

2.1 Generation of the profile and surface of the roller

In this paper, two kinds of roller profiles are utilized for generating the whirl-machining tool profile: cylindrical and conical. Straight lines and fillets generate the tool. The straight lines consist of $\mathbf{r}_1=[x_1,y_1]=[a+u\sin\alpha,b+u\cos\alpha]$, $\mathbf{r}_3=[x_3,y_3]=[u,c]$ and $\mathbf{r}_5=[x_5,y_5]=[-x_1,y_1]$. The fillets consist of $\mathbf{r}_2=[x_2,y_2]=[a-r\cos\alpha+r\cos u,c+r\sin\alpha+r\sin u]$ and $\mathbf{r}_4=[x_4,y_4]=[-x_2,y_2]$. The profile and surface equations of the roller can be expressed as the following equations.

$$\mathbf{r}_A(u)=[x_A,y_A,z_A,1]^T=[x_i(u),0,z_i(u),1]^T,\ i=1\sim 5 \tag{1}$$

$$\mathbf{r}_B(u,\theta)=\begin{bmatrix}x_B\\y_B\\z_B\\1\end{bmatrix}=\begin{bmatrix}1&0&0&0\\0&\cos\theta&\sin\theta&0\\0&-\sin\theta&\cos\theta&0\\0&0&0&1\end{bmatrix}\mathbf{r}_A(u) \tag{2}$$

where a is half of the profile width; u is profile parameter; α is the taper angle; b is tool pitch radius; r is fillet radius; c is the distance between the profile root and the origin point; $\mathbf{r}_B$ is a position vector of a single roller surface; θ is the circumferential parameter of the roller surface; and $\mathbf{r}_A$ is a position vector of the profile of roller. The axial section of the roller profile can be seen in **Fig. 3.** When the tool is cylindrical, the value of the taper angle is equal to zero. On the other hand, the taper angle should be more than zero for the conical tool. The roller profile is in the *xy*-section, while the swivel angle related to the feeding movement of the proposed machine rotates about the *y*-axis. Therefore, in **Eq. (1)**, the profile is necessary to rotate into an *xz*-section to fit with the structure and mechanism of the proposed CNC machine.

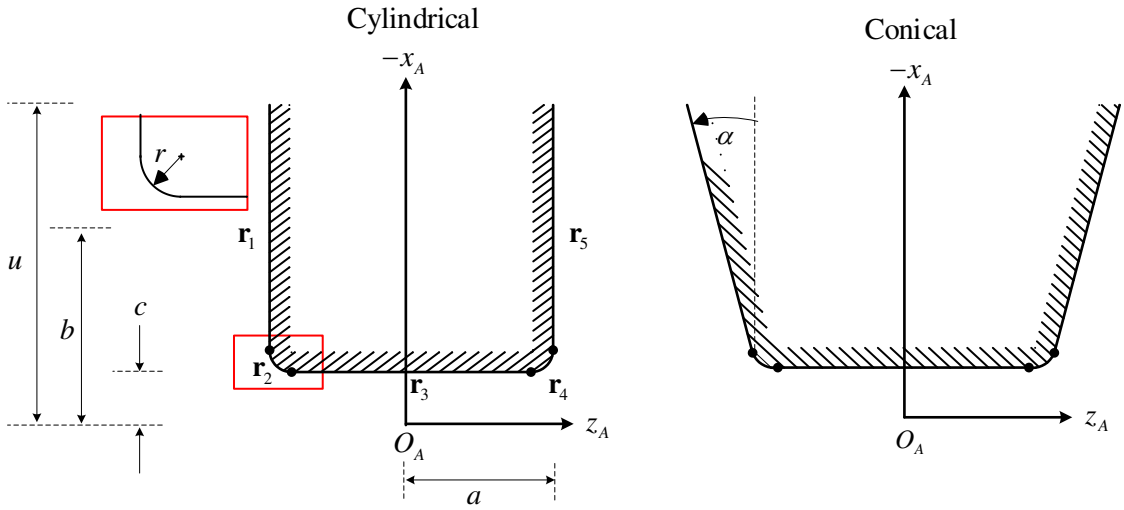

Fig. 3 The roller profile at the axial section

2.2 Generation of the profile and surface of the whirl-machining tool

The whirl-machining process is commonly performed to machine the workpiece in the combination of the rotation of the tool and the workpiece. In the whirl-machining, the lead of the workpiece is controlled by the inclination of the whirl-machining tool concerning the workpiece axis and the feed rate of the whirl-machining tool. The roller-gear cam is identical to the shape of the globoidal worm. Based on the theory of gearing by Litvin [19], the machining method of the roller-gear cam can be seen in **Fig. 4**, which is identical to the generation of globoidal worms. The whirl-machining tool is tilted to generate the lead angle of the thread and is placed eccentric to the workpiece. Therefore, the whirl-machining tool profile is provided from the roller profile, which is projected with an angle the same as the lead angle of the roller-gear cam. The relative position of the roller profile and whirl-machining tool profile can be seen in **Fig. 5** below.

The equations of the whirling tool profile can be provided by **Eq. (3)**. The position vector and the unit normal vector for the whirling tool surface is developed using **Eq. (4)** and **Eq. (5**), respectively. The whirl-machining tool surface can be seen in **Fig. 6**. The 3-D modeling design of the tool can be seen in **Fig. 7** by considering relief and rake angles.

$$\mathbf{r}_C(u)=[x_C,y_C,z_C,1]^T=[x_i(u),0,z_i(u),1]^T,\ i=6\sim 10 \tag{3}$$

$$\mathbf{r}_D(u,\beta)=\begin{bmatrix}x_D\\y_D\\z_D\\1\end{bmatrix}=\begin{bmatrix}\cos\beta&\sin\beta&0&0\\-\sin\beta&\cos\beta&0&0\\0&0&1&0\\0&0&0&1\end{bmatrix}\mathbf{r}_C(u),\ \mathbf{r}_D'=[x_D,y_D,z_D]^T \tag{4}$$

$$\mathbf{n}_D(u,\beta)=\begin{bmatrix} n_{Dx} \\ n_{Dy} \\ n_{Dz} \end{bmatrix}=\frac{\partial_\beta \mathbf{r}'_D \times \partial_u \mathbf{r}'_D}{\left|\partial_\beta \mathbf{r}'_D \times \partial_u \mathbf{r}'_D\right|}=\begin{bmatrix} -x_C z_C \cos\beta \\ x_C z_C \sin\beta \\ x_C \end{bmatrix} \tag{5}$$

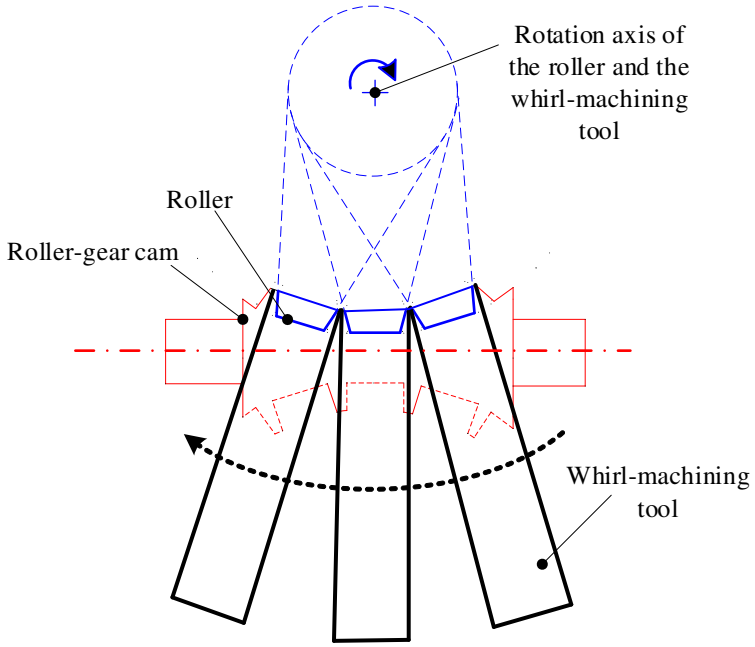

Fig. 4 Process of globoidal shape machining using the whirl-machining tool

where $\mathbf{r}_C$ is a position vector of the whirl-machining tool profile; $[x_6, y_6]=[(a+u\sin\alpha)\cos\lambda, b+u\cos\alpha]$; λ is the angle equal to lead angle of the roller-gear cam; $[x_7, y_7]=[(a-r\cos\alpha+r\cos u)\cos\lambda, c+r\sin\alpha+r\sin u]$; $[x_8, y_8]=[u, c]$; $[x_9, y_9]=[-x_7, y_7]$; $[x_{10}, y_{10}]=[-x_6, y_6]$; β is the circumferential parameter of the whirl-machining tool surface; $\mathbf{r}_D$ is a position vector of the whirl-machining tool surface; and $\mathbf{n}_D$ is the unit normal vector of the whirl-machining tool surface. The whirl-machining tool profile is in the *xy*-section. At the same time, the swivel angle related to the feeding movement of the proposed machine rotates about the *y*-axis. Therefore, the profile is necessary to rotate into an *xz*-section to fit with the structure and mechanism of the proposed CNC machine.

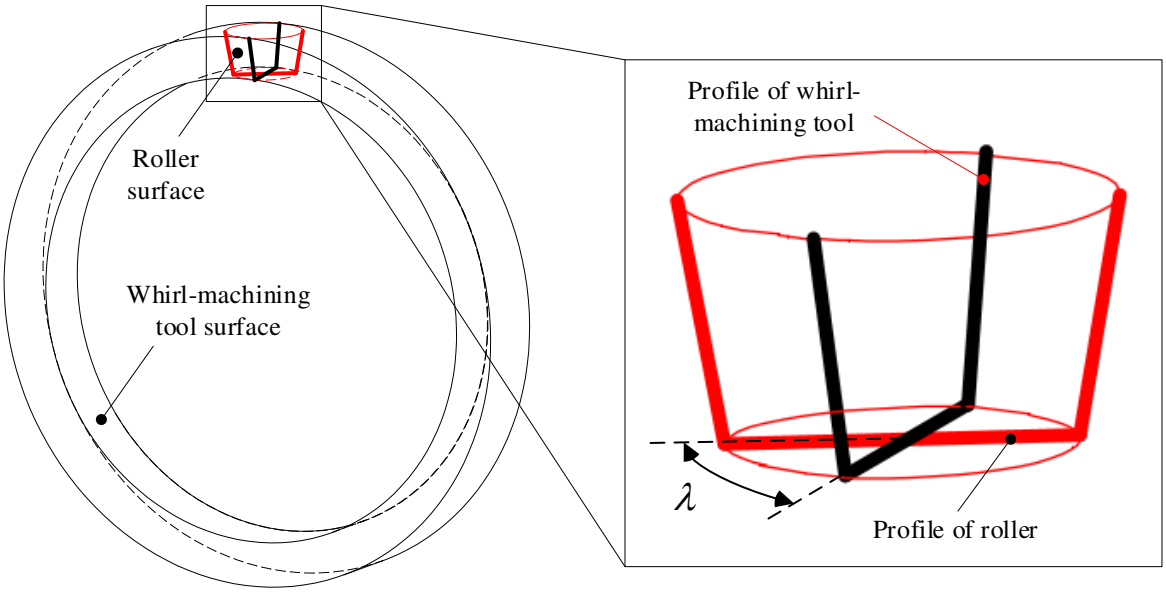

Fig. 5 Relative position of whirl-machining tool profile on the roller profile

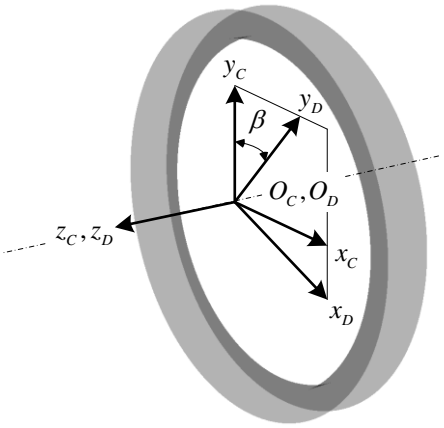

Fig. 6 The whirl-machining tool surface

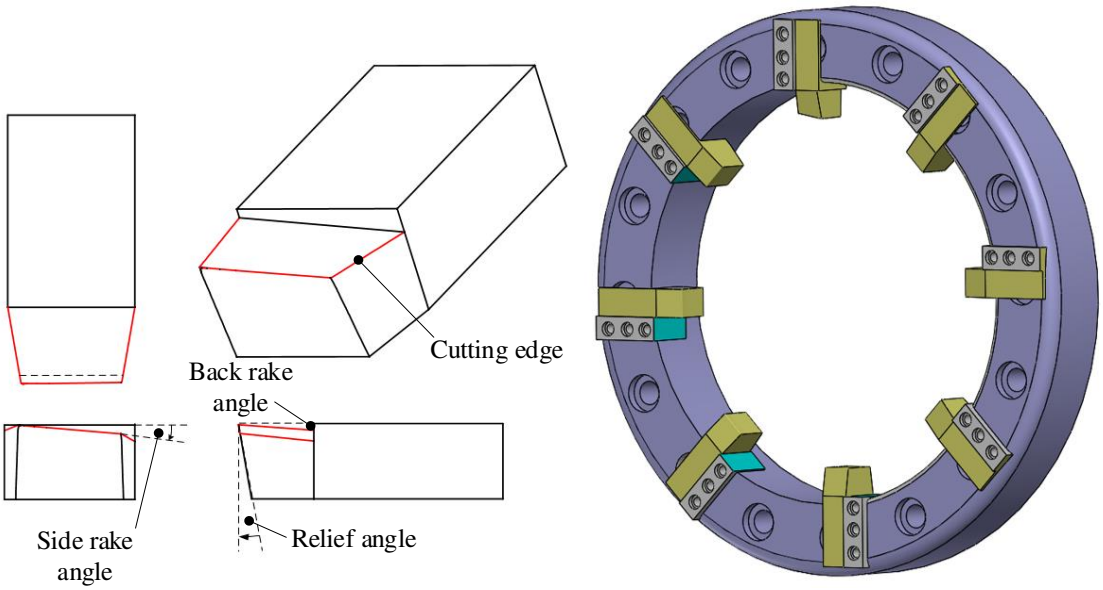

Fig. 7 The 3-D conceptual design of the whirl-machining tool

2.3 Generation of the roller-gear cam surface

A method to generate the roller-gear cam surface has been presented in previous studies [12, 13, 21]. However, the shape of the roller-gear cam in previous studies differs from this paper. Therefore, this paper utilizes the roller profile to generate the cutting tool for generating the roller-gear cam surface. The coordinate system of the cutting tool should be defined before deriving the surface equation of the roller-gear cam. The roller-gear cam surface can be described, based on rigid body transformations, as the swept surfaces of the cutting tool. In terms of studying the motion of a rigid body associated with a different coordinate system, the coordinate transformation is suitable for studying it. The surface equation for the cutting tool is expressed by:

$$\mathbf{r}_E(u,\alpha)=\begin{bmatrix} x_E \\ y_E \\ z_E \\ 1 \end{bmatrix}=\begin{bmatrix} 1 & 0 & 0 & C_1 \\ 0 & 1 & 0 & 0 \\ 0 & 0 & 1 & 0 \\ 0 & 0 & 0 & 1 \end{bmatrix}\begin{bmatrix} 1 & 0 & 0 & 0 \\ 0 & \cos\vartheta & \sin\vartheta & 0 \\ 0 & -\sin\vartheta & \cos\vartheta & 0 \\ 0 & 0 & 0 & 1 \end{bmatrix}\begin{bmatrix} \cos\alpha & \sin\alpha & 0 & 0 \\ -\sin\alpha & \cos\alpha & 0 & 0 \\ 0 & 0 & 1 & 0 \\ 0 & 0 & 0 & 1 \end{bmatrix}\mathbf{r}_C(u) \tag{6}$$

$$=\begin{bmatrix} C_1 + x_i\cos\alpha \\ -x_i\cos\vartheta\sin\alpha + z_i\sin\vartheta \\ x_i\sin\alpha\sin\vartheta + z_i\cos\vartheta \\ 1 \end{bmatrix},\ i=1\sim 5$$

$$\mathbf{n}_E(u,\alpha)=\begin{bmatrix} n_{Ex} \\ n_{Ey} \\ n_{Ez} \end{bmatrix}=\frac{\partial_\alpha \mathbf{r}'_E \times \partial_u \mathbf{r}'_E}{\left|\partial_\alpha \mathbf{r}'_E \times \partial_u \mathbf{r}'_E\right|}=\begin{bmatrix} -x_i z_i \cos\vartheta^2 \cos\alpha - x_i z_i \cos\alpha \sin\vartheta^2 \\ x_i \cos\alpha^2 \sin\vartheta + x_i \sin\alpha^2 \sin\vartheta + x_i z_i \cos\vartheta \sin\alpha \\ x_i \cos\alpha^2 \cos\vartheta + x_i \cos\vartheta \sin\alpha^2 - x_i z_i \sin\alpha \sin\vartheta \end{bmatrix},\ i=1\square 5 \tag{7}$$

where $\mathbf{r}_E$ is a position vector of the cutting tool surface; $\mathbf{r}'_E=[x_E, y_E, z_E]^T$; C_1 is the distance between the roller-gear cam and the cutting tool; ϑ is the setting angle of the cutting tool; α is the surface parameter of the cutting tool; and $\mathbf{n}_E$ is a unit normal vector of the cutting tool.

According to the theory of gearing [19], the roller-gear cam surface equation can be achieved by considering the locus of the cutting tool surface [13]. The equation can be represented in the roller-gear cam coordinate system and the meshing equation of the roller-gear cam with the cutting tool.

The relative motion between the cutting tool surface and the roller-gear cam can be seen in **Fig. 8**. Coordinate systems $S_E(x_E, y_E, z_E)$ and $S_F(x_F, y_F, z_F)$ correspond to the cutting tool surface and the roller-gear cam, respectively. Therefore, the coordinate system $S_1(x_1, y_1, z_1)$ and $S_2(x_2, y_2, z_2)$ are connected rigidly to the cutting tool surface and the roller-gear cam, respectively.

The coordinate system $S_1(x_1, y_1, z_1)$ of the cutting tool rotates about the y_1 axis Through an angle ε. The coordinate system $S_2(x_2, y_2, z_2)$ of the roller-gear cam rotates about the z_2 axis through an angle γ. The relationship between the two angles is $\varepsilon=\gamma/z$, where z is the number of the roller.

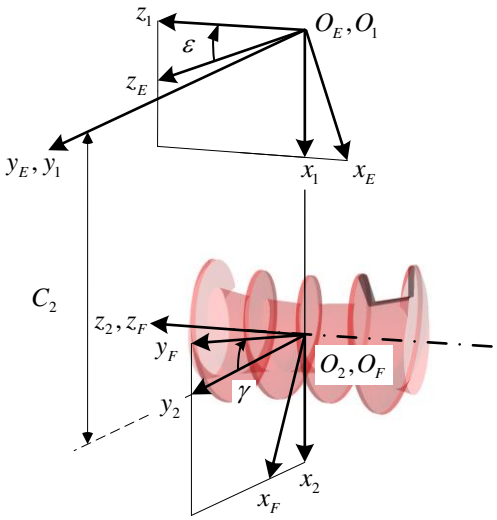

Fig. 8 Coordinate system for roller-gear cam generation

The position vector for the trajectory of the cutting tool surface, represented in the coordinate system $S_F(x_F, y_F, z_F)$, is expressed by:

$$\mathbf{r}_F(u,\alpha,\gamma)=\begin{bmatrix} x_F \\ y_F \\ z_F \\ 1 \end{bmatrix}=\mathbf{M}_{FE}(\omega_2)\mathbf{r}_E(u,\alpha)=\begin{bmatrix} -C_2\cos\gamma + x_E\cos\varepsilon\cos\gamma + z_E\cos\gamma\sin\varepsilon + y_E\sin\gamma \\ y_E\cos\gamma + C_2\sin\gamma - x_E\cos\varepsilon\sin\gamma - z_E\sin\varepsilon\sin\gamma \\ z_E\cos\varepsilon - x_E\sin\varepsilon \\ 1 \end{bmatrix} \tag{8}$$

$$\mathbf{M}_{FE}=\begin{bmatrix} \cos\varepsilon\cos\gamma & \sin\gamma & \cos\gamma\sin\varepsilon & -C_2\cos\gamma \\ -\cos\varepsilon\sin\gamma & \cos\gamma & -\sin\varepsilon\sin\gamma & C_2\sin\gamma \\ -\sin\varepsilon & 0 & \cos\varepsilon & 0 \\ 0 & 0 & 0 & 1 \end{bmatrix}$$

$$\mathbf{n}_F(u,\alpha,\gamma)=\begin{bmatrix} n_{Fx} \\ n_{Fy} \\ n_{Fz} \end{bmatrix}=\mathbf{L}_{FE}(\gamma)\mathbf{n}_E(u,\alpha)=\begin{bmatrix} n_{Ex}\cos\varepsilon\cos\gamma + n_{Ez}\cos\gamma\sin\varepsilon + n_{Ey}\sin\gamma \\ n_{Ey}\cos\gamma - n_{Ex}\cos\varepsilon\sin\gamma - n_{Ez}\sin\varepsilon\sin\gamma \\ n_{Ez}\cos\varepsilon - n_{Ex}\sin\varepsilon \end{bmatrix} \tag{9}$$

$$f_F(u,\alpha,\gamma)=\mathbf{n}_F\cdot\partial_\gamma\mathbf{r}'_F=y_E n_{Ex}\cos\alpha+y_E n_{Ez}\sin\varepsilon+n_{Ey}(C_2-x_E\cos\varepsilon-z_E\sin\varepsilon)=0 \tag{10}$$

where $\mathbf{M}_{FE}$ is the transformation matrix from S_E to S_F; $\mathbf{L}_{FE}$ is the 3×3 upper left submatrix of $\mathbf{M}_{FE}$; $\mathbf{r}_F$ is the position vector for the trajectory of cutting tool surface; $\mathbf{r}'_F=[x_F,y_F,z_F]^T$; $\mathbf{n}_F$ is the unit normal vector of the tool surface locus; f_F is the meshing equation; γ is the rotation angle of the coordinate system S_F; ε is the rotation angle of the coordinate system S_E; and C_2 is the center distance between the coordinate system S_F and the coordinate system S_E, that equals the total distance between the roller and the roller-gear cam at the throat. Furthermore, by simultaneously considering **Eqs. (8)** and **(10)**, the mathematical model of the surface of the roller-gear cam can be obtained. The roller-gear cam surface and roller surface can be seen in **Fig. 9**, where the clearance and the backlash are not considered.

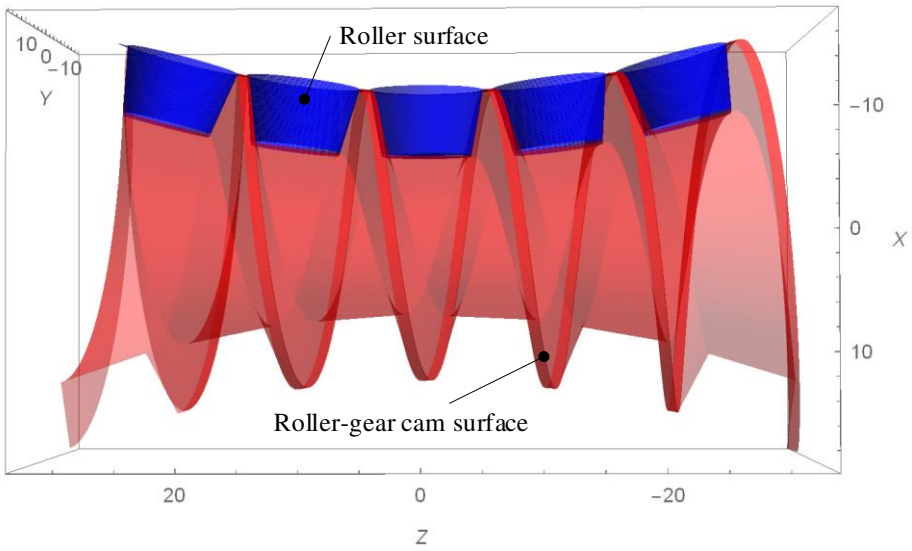

Fig. 9 Roller-gear cam and roller surfaces

4. Mathematical model for generating the roller-gear cam surface on the whirl-machining tool

4.1 Coordinate system and machine setting

The whirl-machining tool, powered by a motor and rotates at high speed, performs the cutting motion in the whirl-machining process [2]. Four motions occur in the process: the rotation of the workpiece, the rotation of the whirl-machining tool, the feeding motion of the whirl-machining tool, and the radial translation of the tools [8]. The coordinate system and motion diagram based on the CNC machine for this study can be seen in **Fig. 10**.

The machine consists of three sliding axes (X, Y, and Z) and four rotation axes (A, B, C, and D). The *x*-axis is the axis of axial sliding of the whirl-machining tool; the *y*-axis is the axis of tangential sliding of the whirl-machining tool; and the *z*-axis is the axis of radial sliding of the whirl-machining tool. A is the feeding spindle axis; B is the tool rotation axis; C is the tool spindle axis; and D is the workpiece spindle axis. A, C, and D are motions to generate the roller-gear cam surface; while X, Y, Z, and B control the whirl-machining tool position.

The coordinate system in **Fig. 10** is utilized for generating the coordinate transformation matrix M_{GD} of the roller-gear cam coordinate system S_G, which is transformed from a whirl-machining tool coordinate system S_D on a CNC machine as follows:

$$\mathbf{M}_{GD}=\mathbf{M}_{G6}\mathbf{M}_{65}\mathbf{M}_{54}\mathbf{M}_{43}\mathbf{M}_{3D} \tag{11}$$

$$\mathbf{M}_{G6}=\begin{bmatrix}\cos\psi & \sin\psi & 0 & 0\\ -\sin\psi & \cos\psi & 0 & 0\\ 0 & 0 & 1 & 0\\ 0 & 0 & 0 & 1\end{bmatrix};\mathbf{M}_{65}=\begin{bmatrix}1 & 0 & 0 & -C_x\\ 0 & 1 & 0 & C_y\\ 0 & 0 & 1 & -C_z\\ 0 & 0 & 0 & 1\end{bmatrix};\mathbf{M}_{54}=\begin{bmatrix}\cos\sigma & 0 & \sin\sigma & 0\\ 0 & 1 & 0 & 0\\ -\sin\sigma & 0 & \cos\sigma & 0\\ 0 & 0 & 0 & 1\end{bmatrix};$$

$$\mathbf{M}_{43}=\begin{bmatrix}1&0&0&C_3\\0&1&0&0\\0&0&1&0\\0&0&0&1\end{bmatrix};\mathbf{M}_{3D}=\begin{bmatrix}1&0&0&0\\0&\cos\omega&\sin\omega&0\\0&-\sin\omega&\cos\omega&0\\0&0&0&1\end{bmatrix}$$

where $\mathbf{M}_{GD}$ is the transformation matrix from the coordinate system of the whirl-machining tool S_D to the coordinate system of the roller-gear cam S_G based on the proposed CNC machine; ψ is the rotation angle of the roller-gear cam spindle (D); σ is an angle of the rotation feeding (A); ω is the whirl-machining tool setting angle about the *x*-axis (B); C_3 is the total distance between feeding rotation center and whirl-machining tool; C_x is the sliding feed of the *x*-axis/horizontal slide (1); C_y is the sliding feed of the *y*-axis/vertical slide (Y); and C_z is the sliding feed of the *z*-axis/whirling arm slide (Z). The mechanical setup of each axis can be expressed as follows:

$$\begin{cases}\omega=\vartheta\\ \sigma=\varepsilon\\ \psi=\gamma\\ C_x=C_3\cos\sigma+(C_2-C_1\cos\varepsilon)\cos(\gamma-\psi)\\ C_y=(C_2-C_1\cos\varepsilon)\sin(\gamma-\psi)\\ C_z=C_1\sin\varepsilon-C_3\sin\sigma\end{cases}\tag{12}$$

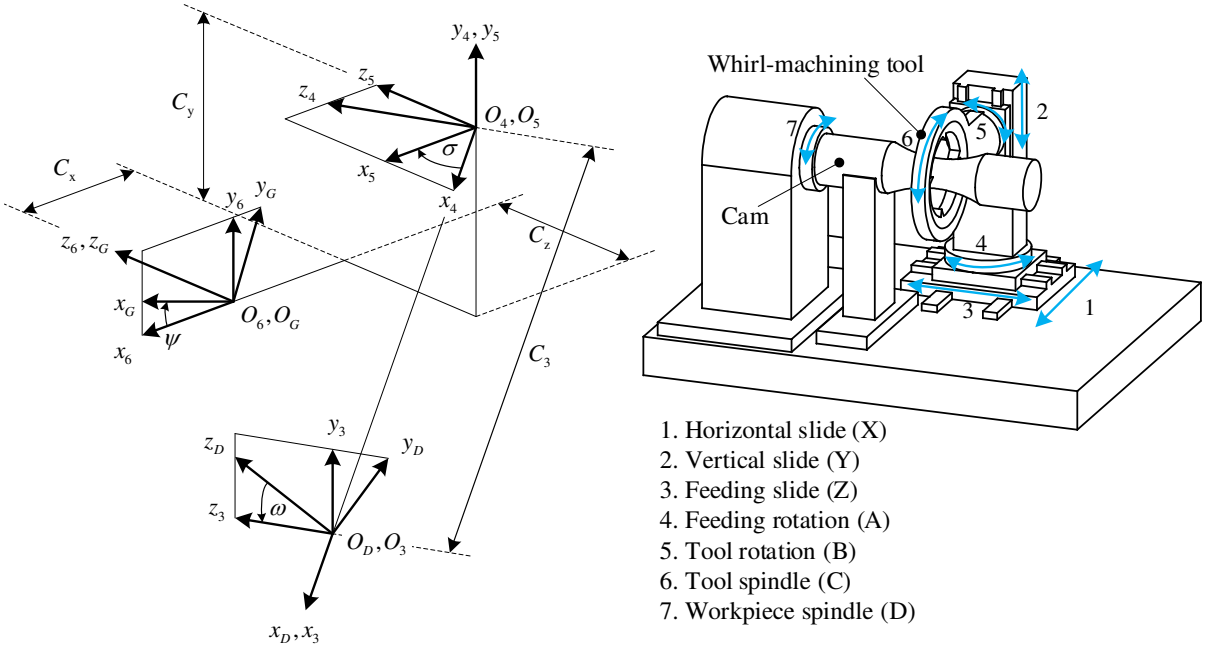

Fig. 10 Coordinate system and structure of the proposed machine

The coordinate system in **Fig. 10** is a machining coordinate system of the whirl-machining tool, which can be utilized to conduct a cutting simulation of a roller-gear cam with the whirl-machining tool in the proposed multi-axis CNC machine. The equation of the whirl-machining tool trajectory and its unit normal vector can be obtained as follows:

$$\mathbf{r}_G(u,\beta,\psi)=\begin{bmatrix}x_G\\y_G\\z_G\\1\end{bmatrix}=\mathbf{M}_{GD}(\psi)\mathbf{r}_D(u,\beta)=\begin{bmatrix}h_1+z_D(\cos\omega\cos\psi\sin\sigma+\sin\omega\sin\psi)\\h_2+z_D(\cos\psi\sin\omega-\cos\omega\sin\sigma\sin\psi)\\-C_z-C_3\sin\sigma-x_D\sin\sigma+z_D\cos\omega\cos\sigma\\1\end{bmatrix},\tag{13}$$

$$h_1 = -C_x\cos\psi + C_3\cos\sigma\cos\psi + C_y\sin\psi + x_D\cos\sigma\cos\psi,$$
$$h_2 = C_y\cos\psi + C_x\sin\psi - C_3\cos\sigma\sin\psi - x_D\cos\sigma\sin\psi,$$

$$\mathbf{n}_G(u,\beta,\psi) = \begin{bmatrix} n_{Gx} \\ n_{Gy} \\ n_{Gz} \end{bmatrix} = \mathbf{L}_{GD}(\psi)\mathbf{n}_D(u,\beta) = \begin{bmatrix} g_1 + n_{Dz}(\cos\omega\cos\psi\sin\sigma + \sin\omega\sin\psi) \\ g_2 + n_{Dy}(\cos\omega\cos\psi + \sin\omega\sin\sigma\sin\psi) \\ n_{Dz}\cos\omega\cos\sigma - n_{Dy}\cos\sigma\sin\omega - n_{Dx}\sin\sigma \\ 1 \end{bmatrix}, \tag{14}$$
$$g_1 = n_{Dx}\cos\sigma\cos\psi + n_{Dy}(-\cos\psi\sin\omega\sin\sigma + \cos\omega\sin\psi),$$
$$g_2 = -n_{Dx}\cos\sigma\sin\psi + n_{Dz}(\cos\psi\sin\omega - \cos\omega\sin\sigma\sin\psi),$$

where $\mathbf{r}_G$ is the a position vector of whirl tool machining locus; $\mathbf{n}_G$ is the unit normal vector of whirl tool locus; and $\mathbf{L}_{GD}$ is the 3×3 upper left submatrix of $\mathbf{M}_{GD}$. Contact point can be obtained when the normal vectors perpendicular to the direction of the relative velocity from two curves of related motions. Furthermore, the meshing equation can be obtained as follows:

$$f_G(u,\beta,\psi) = \mathbf{n}_G \cdot \partial_\psi \mathbf{r}'_G = n_{Dz}g_{11} + n_{Dx}\cos\sigma(C_y + z_D\sin\omega) + n_{Dy}(g_{12} - g_{13}) = 0, \tag{15}$$
$$g_{11} = (C_x - C_3\cos\sigma)\sin\omega + C_y\cos\omega\sin\sigma - x_D\cos\sigma\sin\omega,$$
$$g_{12} = C_x\cos\omega - C_3\cos\omega\cos\sigma,$$
$$g_{13} = C_y\sin\omega\sin\sigma - x_D\cos\omega\cos\sigma - z_D\sin\sigma,$$

where f_G is the equation of meshing equation of the generated point and $\mathbf{r}'_G = [x_G, y_G, z_G]^T$.

4.2 Normal deviation in the roller-gear cam surface

The proposed mathematical model is utilized to calculate the points on the roller-gear cam surface, which is generated by the whirl-machining tool. The original theoretical roller-gear cam surface generates a datum surface for determining the deviation and cutting precision in the normal direction. **Fig. 11** shows that the roller-gear cam surface is divided into seven axial profile sections. The sections are based on the input value of γ. The range input value is from 3π to -3π. The cutting simulation of the whirl-machining tool provides cutting points or generated points on these sections. A single profile on one section consists of 160 points. The normal deviation for each point is calculated as:

$$(\mathbf{r}_F + \mathbf{n}_F\delta_F) - \mathbf{r}_G = 0 \tag{16}$$

where δ_F is the normal deviation; and $\mathbf{n}_F$ is the unit normal vector of the roller-gear cam surface.

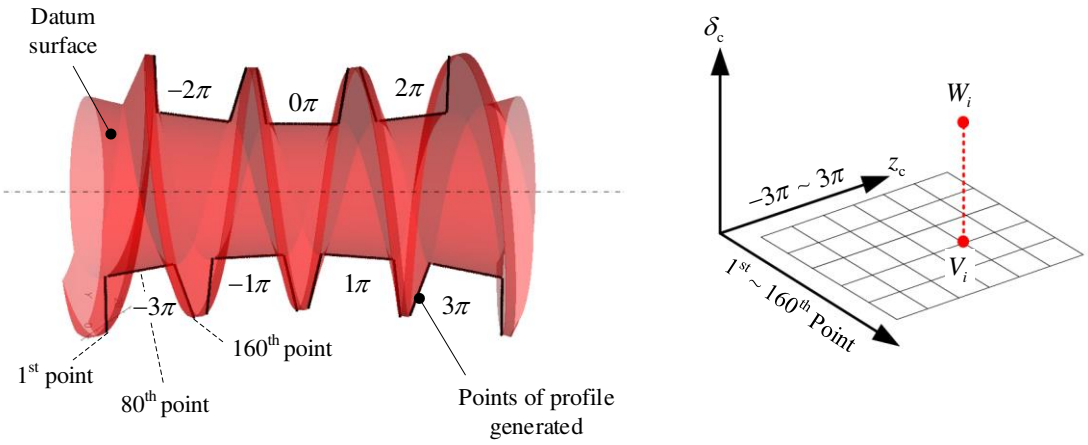

Fig. 11 Normal deviations on the roller-gear cam surface

A zero normal deviation on the datum surface can be seen in **Fig. 11** at the point V_i, where $\mathbf{r}_F$ is the vector of its position, and $\mathbf{n}_F$ is the vector of its unit normal. A point W_i is a point that is not on the datum

surface, this point is labeled as the generated point. From the point W_i to the V_i, the minimum distance must be in the same direction as the normal vector. A surface topology coordinate was proposed to compare the distance between the datum and generated roller-gear cam. The distances are labeled as normal deviation. Coordinate of the surface topology was developed into $[\text{Points}, \delta_c, z_c]$.

5. Numerical examples

Due to its high productivity and quality characteristics, the whirl-machining process is widely used in the machining of helical shape workpieces, where the cutting motion in the process is performed by the tool ring, which is powered by a motor and rotated at high speed [1, 2]. Compared to turning, whirling has advantages in surface finish, tool wear, and chip control because the material is removed in a small volume at a high cutting speed [11].

The numerical examples validate the proposed mathematical model for whirling a roller-gear cam. Based on a theoretical point of view, the generated roller-gear cam surface should coincide with the datum of the roller-gear cam surface. However, errors may occur due to the curve fitting and numerical approaches [29]. In this case, a whirl-machining tool was utilized to machine a roller-gear cam of RGC drive to observe if the proposed mathematical model could attain the requisite numerical accuracy. Design parameters in the examples can be seen in **Table 1**. The 3-D coordinate system of the cutting line is listed in **Table 2** (16 points from 160 points). The 2-D coordinate system of the generated roller-gear cam profile at the axial section is listed in **Table 3** (16 points from 160 points).

Table 1. Design parameters for the numerical examples

Parameters, symbols (units)	Values		
	Numerical example 1	Numerical example 2	
Roller-gear cam type	Globoidal	Globoidal	Cylindrical
Roller type	Cylindrical	Conical	Conical
Taper angle, α (°)	0	10	10
Length of tool root, a (mm)	9/5	9	9
Lead angle, λ (°)		10	
Tool pitch radius, b (mm)		40	
Length of the roller-gear cam (mm)		44	
Distance, c (mm)		37	
Center distance, C_1 (mm)		100	
Center distance, C_2 (mm)		100	
Center distance, C_3 (mm)		130	
Radius of the fillet, r (mm)		0.5	
Number of the roller, z (pieces)		50	
Whirl-machining tool pitch radius (mm)		40	

Table 2. Position coordinates of points on the cutting line

Generated points	Coordinates of points		
	x	y	z
1	-12.60	4.54	-5.82
2	-10.92	1.51	-4.94
3	-9.00	-1.79	-4.01
4	-7.01	-2.37	-3.56
5	-6.79	-0.89	-3.71
6	-6.64	-0.15	-3.66
7	-6.58	0.17	-3.48
8	-6.60	0.11	-1.17
9	-6.60	-0.10	1.17
10	-6.59	-0.18	3.48
11	-6.64	0.12	3.67
12	-6.79	0.95	3.70
13	-6.97	2.25	3.56
14	-9.00	1.78	4.01
15	-10.92	-1.51	4.93
16	-12.60	-4.53	5.82

Table 3. Coordinate system of the generated roller-gear cam profile at $\gamma = 0$

Generated points	2-D coordinate system							
	Numerical example 1				Numerical example 2			
	$a = 9$		$a = 5$		Globoidal conical		Cylindrical conical	
	x	z	x	z	x	z	x	z
1	-12.99	-4.5	-12.99	-2.5	-12.95	-5.02	-12.95	-5.02
2	-10.99	-4.5	-10.99	-2.5	-10.98	-4.67	-10.98	-4.67
3	-8.99	-4.5	-8.99	-2.5	-9.01	-4.33	-9.01	-4.33
4	-6.99	-4.5	-6.99	-2.5	-7.04	-3.98	-7.04	-3.98
5	-6.74	-4.43	-6.74	-2.43	-6.78	-3.87	-6.78	-3.87
6	-6.56	-4.25	-6.56	-2.25	-6.63	-3.68	-6.63	-3.68
7	-6.49	-3.76	-6.49	-2.03	-6.58	-3.46	-6.58	-3.46
8	-6.50	-1.25	--6.50	-0.67	-6.60	-1.15	-6.59	-1.15
9	-6.50	1.25	-6.50	0.67	-6.60	1.15	-6.59	1.15
10	-6.49	3.76	-6.49	2.03	-6.58	3.46	-6.58	3.46
11	-6.56	4.25	-6.56	2.25	-6.63	3.68	-6.63	3.68
12	-6.74	4.43	-6.74	2.43	-6.78	3.87	-6.78	3.87
13	-6.99	4.5	-6.99	2.5	-7.04	3.98	-7.04	3.98
14	-8.99	4.5	-8.99	2.5	-9.01	4.33	-9.01	4.33
15	-10.99	4.5	-10.99	2.5	-10.98	4.67	-10.98	4.67
16	-12.99	4.5	-12.99	2.5	12.95	5.02	-12.95	5.02

As shown in **Fig. 12**, the datum roller-gear cam and whirl-machining tool are assembled and simulated. The whirl-machining tool surface is located at the relative position of the roller-gear cam, and it fits the roller-gear cam surface. The proposed mathematical model calculates a single cutting line and locus of cutting lines (200). The cutting line is projected as a collection of instant contact points between the surfaces of the roller-gear cam and the whirl-machining tool, although it may more accurately reflect the machining result on the machined roller-gear cam surface. The cutting simulation result shows that the generated roller-gear cam profile, calculated by the simulation, closely fits along the datum roller-gear cam surface.

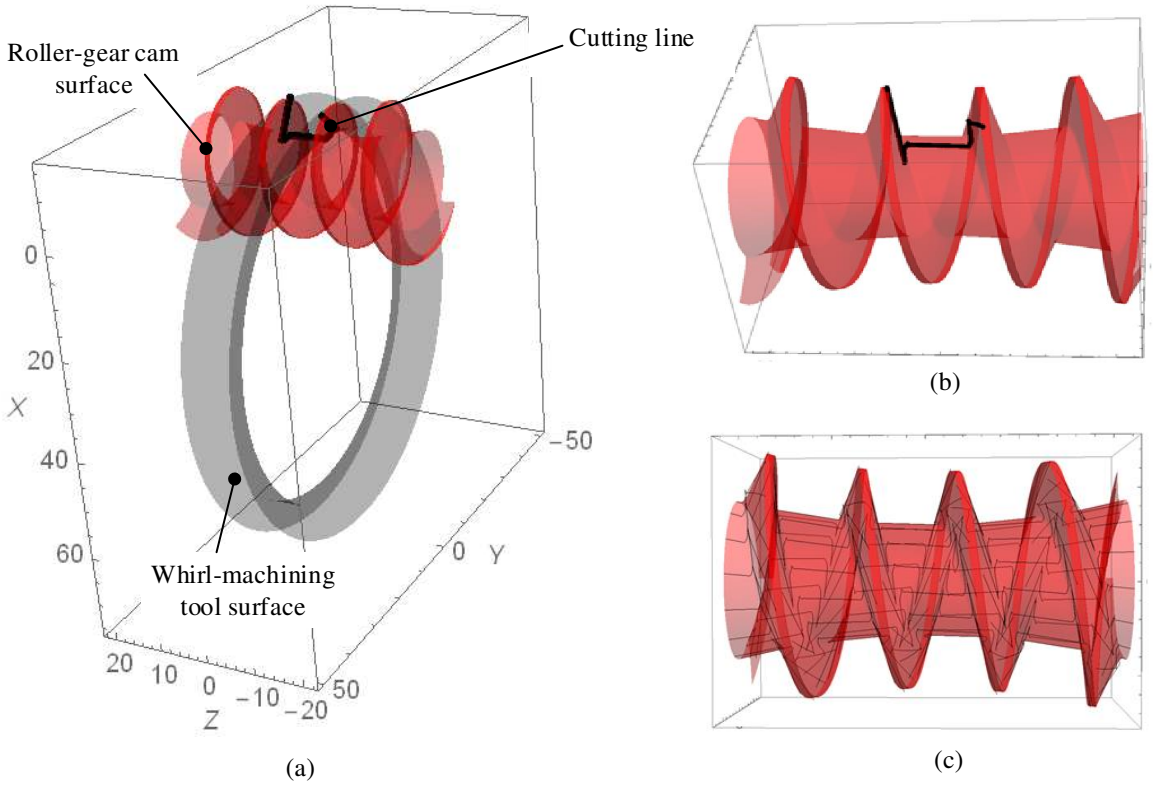

Fig. 12 Cutting simulation result: (a) assembly of tool and roller-gear cam, (b) single generated cutting line, and (c) trajectory of cutting line over the roller-gear cam

5.1 Normal deviations for globoidal roller-gear cam with cylindrical roller

The type of roller-gear cam is globoidal, while the roller is cylindrical. The roller-gear cam has a lead angle of 10 degrees and a length of 44 mm. The tool has a pitch radius of 40 mm, and a root length of 9 and 5 mm. The distance between the tool root and the origin point is 37 mm. The center distance between the roller-gear cam and the tool is 100 mm, the center distance between the roller-gear cam and the roller is 100, and the center distance between the tool and the rotational feeding center is 120 mm. The roller has a number of 50 pieces. The pitch radius of the whirl-machining tool is 40 mm. The normal deviations in **Fig. 13** were obtained by comparing the generated roller-gear cam profile and the datum roller-gear cam profile. **Fig. 14** and **Fig. 15** show the surface topology of two different roller-gear cam surfaces. In this case, the simulations are conducted with two different lengths of tool roots.

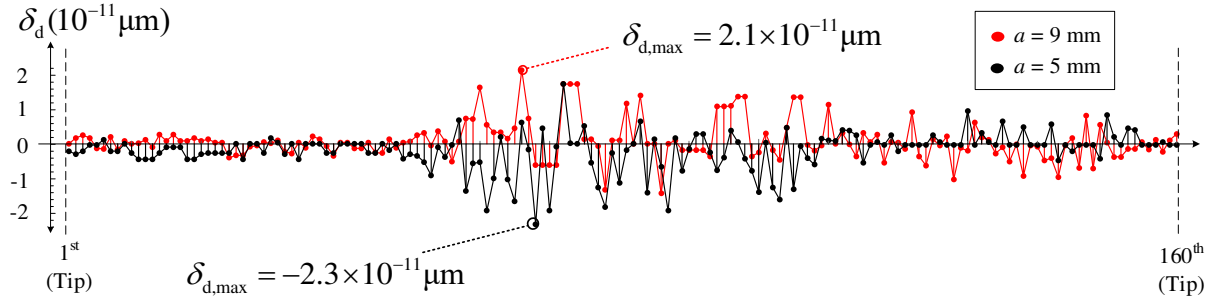

Fig. 13 Normal deviations of the globoidal roller-gear cam with different cylindrical rollers

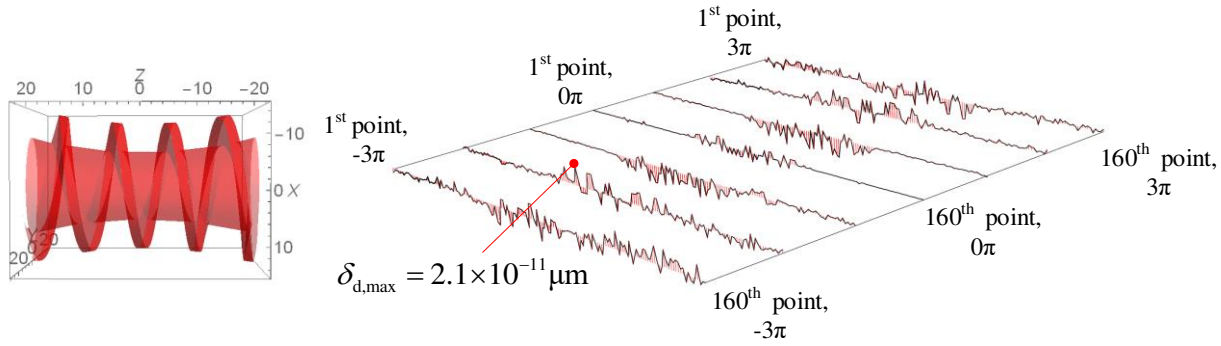

Fig. 14 Surface topologies of globoidal roller-gear cam and cylindrical roller with the length of tool root of 9mm

In order to further understand the precision of the machined roller-gear cam surface, each sectional profile of the machined roller-gear cam is compared with the datum roller-gear cam surface in the normal deviation; thus, the surface topology can be achieved as shown in **Fig. 14** and **Fig. 15**. The figures show the maximal deviations for two different roller-gear cams with the value of 2.1×10^{-11} μm and -2.3×10^{-11} μm, respectively. As a result, the proposed mathematical model is validated, and the whirl-machining process of the roller-gear cam is proved to be practical for different roller-gear cam geometries in this example.

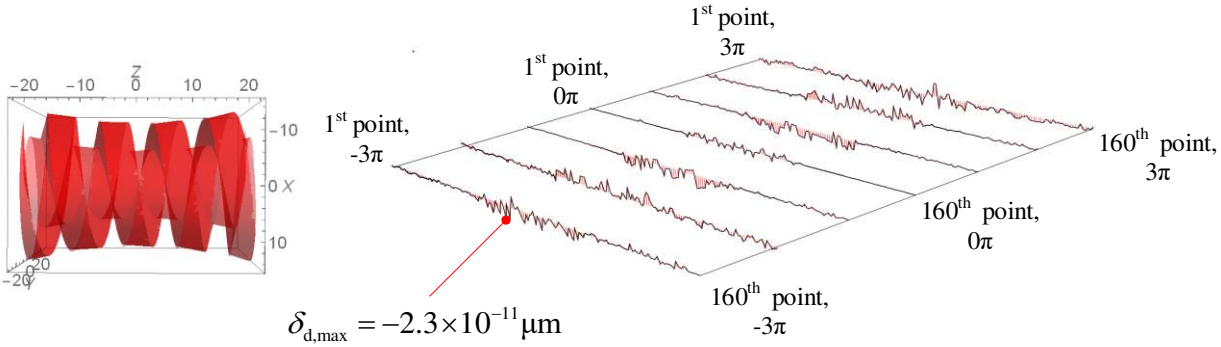

Fig. 15 Surface topologies of globoidal roller-gear cam and cylindrical roller with the length of tool root of 5mm

5.2 Globoidal roller-gear cam with conical roller and conical roller with cylindrical roller-gear

The machinery equipment industry has widely utilized the whirl-machining process to produce helical shape workpieces from difficult-to-machine material for transmissions [3]. The goal of whirling process

simulation is to have better knowledge of the surface generation process and roller-gear cam geometry. In order to spread the accuracy of the proposed model, in this section, the type of roller-gear cam is globoidal with the conical roller shape utilized. The conical shape of the roller can be achieved by giving a value in the taper angle equation. The simulation result for a globoidal roller-gear cam with a conical roller can be seen in **Fig. 16**. The maximum normal deviation that can be achieved is 2.3×10^{-11} µm (**Fig. 17**). The same as the cylindrical roller, the normal deviations of the conical roller approaches zero. The result from the cutting simulation shows that RGC with globoidal roller-gear cam and conical roller able be manufactured using the proposed method.

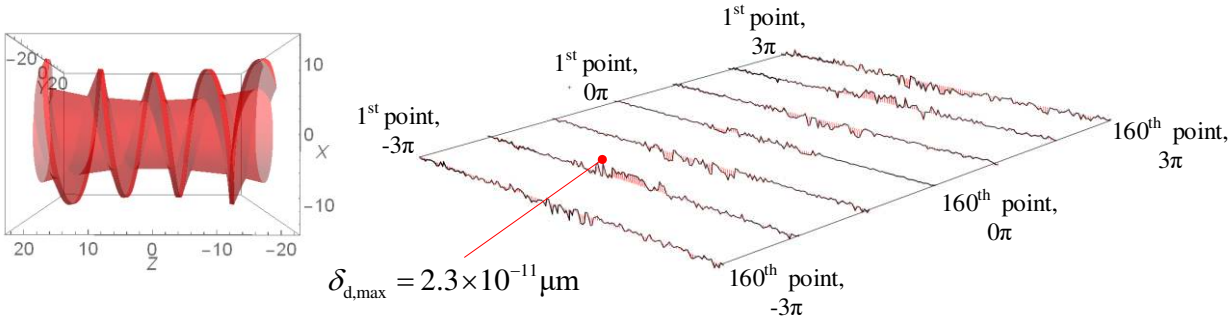

Fig. 16 Surface topology of the globoidal roller-gear cam with conical roller

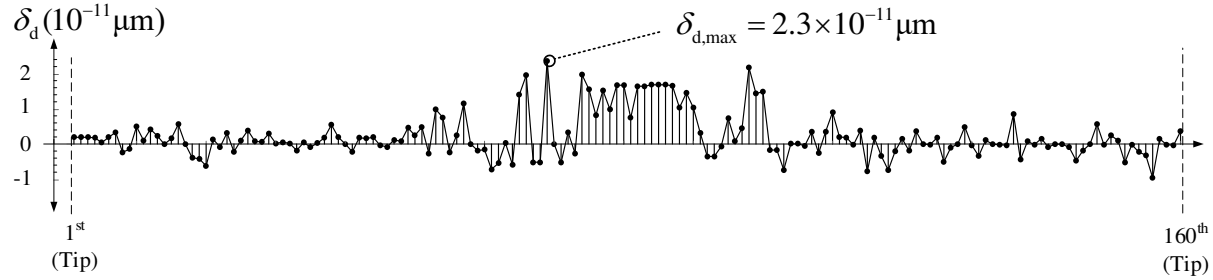

Fig. 17 Normal deviations of the globoidal roller-gear cam with a conical roller

Whirl-machining process is typically utilized to manufacture workpieces by combining tool and workpiece rotations. There are four types of rotational and translational motions in the process: workpiece rotation motion, tool rotation motion, tool axial feed motion, and tool radial translation motion [5, 8]. In addition, in this section, the type of roller-gear cam is cylindrical, while the roller is conical. Cylindrical roller-gear cam mechanisms are widely used in machinery applications such as rotary indexing tables, packing machines, knitting machines, and elevators, which have smaller sizes and higher driving torque than other cam mechanisms. The surface topology of the cylindrical roller-gear cam from the cutting simulation can be seen in **Fig. 18**. The maximum value of normal deviation is -1.4×10^{-11} µm (**Fig. 19**). The result shows that the whirl-milling process is able to manufacture cylindrical roller-gear cam precisely.

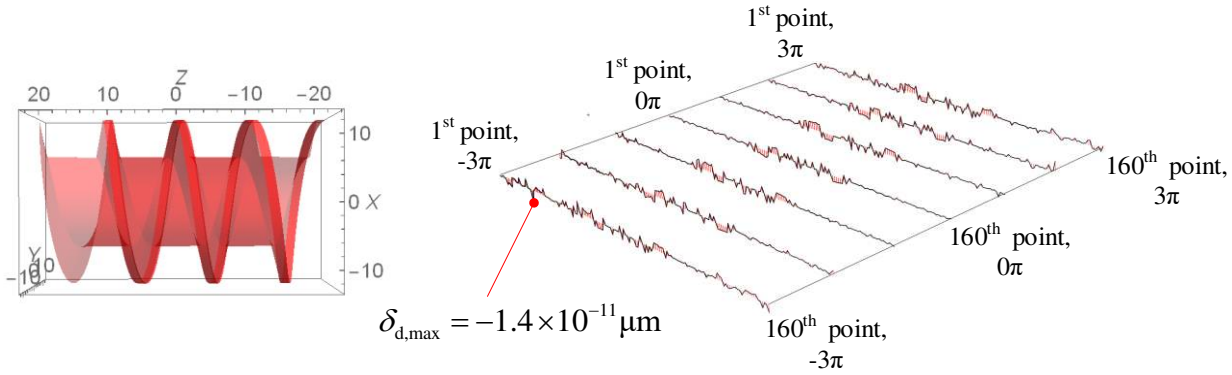

Fig. 18 Surface topology of the cylindrical roller-gear cam with a conical roller

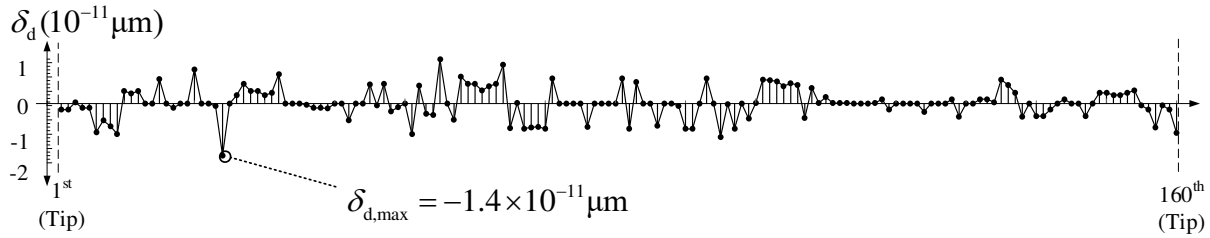

Fig. 19 Normal deviations of the cylindrical roller-gear cam with a conical roller

5.3 The conjugation of the roller and the roller-gear cam

In this section, generated roller profile was obtained from the trajectory of the roller-gear cam **(Fig. 20**). The red lines are the roller profiles and the blue lines are the locus of the roller-gear cam. Compared with conventional workpiece machining processes (grinding, turning, and milling), whirl-machining processes produce a high material removal rate and minimize cutting forces due to their smooth and tangential cutting motions. At the same time, it is regarded as an advanced cutting process that has gradually gained popularity [9, 10]. The basis for the development of differential geometry is a theory of surface. In the gear transmission field, the theory is known as the geometry theory of conjugate surfaces. Conjugation of two surfaces is explained as surfaces that keep continuous and tangent contact. The total power and motion qualities of a gear drive are substantially influenced by the operational performance of conjugate surfaces. Therefore, the conjugation between both roller-gear cam and roller is achieved.

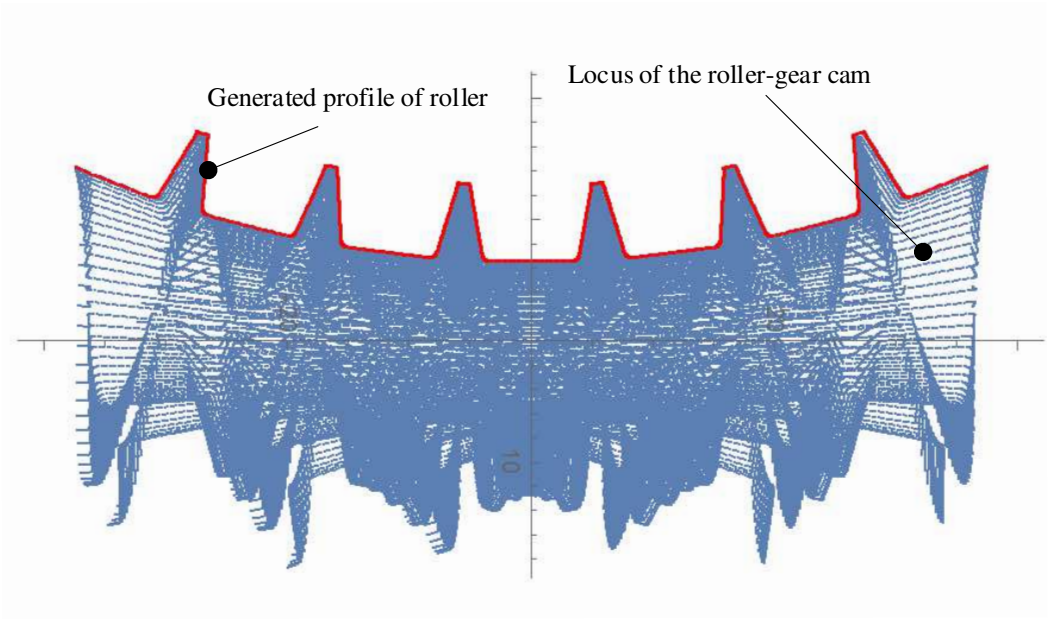

Fig. 20 Generation process of the generated rollers

5.4 Virtual cutting verification

Simulation of the whirl-machining process on the roller-gear cam using the VERICUT (by CGTECH) is conducted. The whirl-machining tool profile, generated from the proposed model using mathematical modeling from numerical example 2, is imported into CAD software to construct a 3-D tool model. The roller-gear cam and the proposed machine structure are generated into a CAD model. Furthermore, the tool, the roller-gear cam, and the machine structure are imported into VERICUT. The proposed machine structure, mechanical setup settings, and the coordinate system in **Fig. 10** are utilized to create the G-code. The virtual cutting process can be seen in **Fig. 21**. The results can be seen in **Fig. 22.** Mathematical modeling (**Fig. 22a)** and virtual cutting simulation (**Fig. 22b)** results of the roller-gear cam are compared**.** The roller-gear cam shape of both results presents an identical result, which is globoidal. The globoidal shape occurs in order to the motion of the swivel angle in the proposed machine. The results show that the mathematical model and virtual machining cutting simulations confirm the kinematics relationship on tool-workpiece interaction. Consequently, the tool design is fully functional.

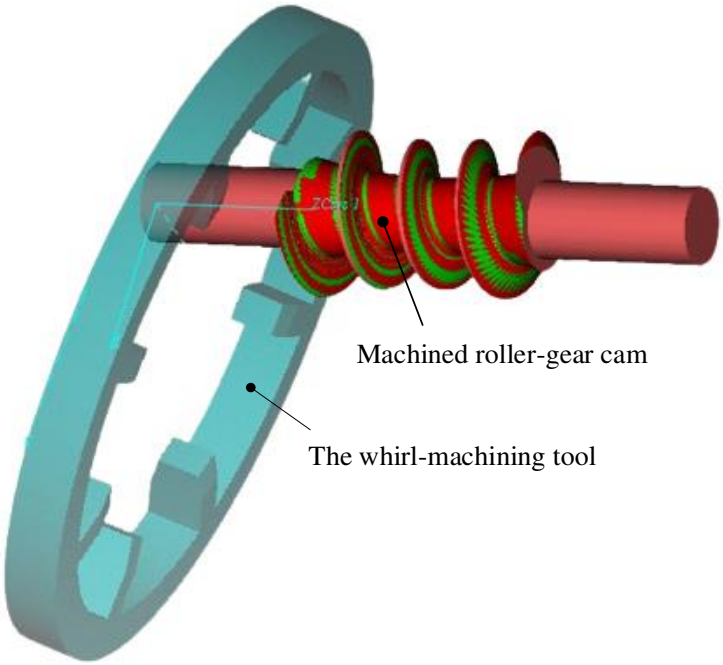

Fig. 21 Virtual cutting simulation process

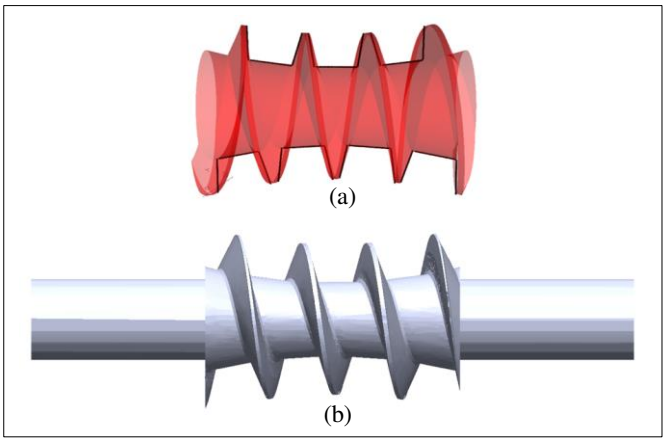

Fig. 22 Cutting simulation results: (a) Mathematical modeling; and (b) Virtual machining

6. Conclusion

In this paper, the main goal of the current study was to propose the technique of manufacturing A roller-gear cam with a whirl-machining tool. Mathematical expressions for roller-gear cam surface, roller surface, and whirl-machining tool are derived. The mathematical model is based on the theory of gearing, differential geometry, and coordinate transformation matrixes. Basic equations tool coordinates and direction for obtaining the mechanical setup parameter are derived. Several numerical examples are conducted to verify the model. The findings indicate that the results obtained from the cutting simulation are compared with theoretical data. The study has shown that the normal deviations approach zero. A virtual cutting simulation was conducted and showed a good result. The model is also used to study the conjugation on roller-gear cam and rollers. The study contributes to our understanding that the proposed method can be applied effectively for manufacturing roller-gear cam by utilizing the whirl-machining process. The absence of experimental investigation limited this study. Therefore, further machining experimentation and meshing test investigation are strongly recommended.

Acknowledgments

The authors express gratitude to the Ministry of Science and Technology in Taiwan for its financial support under project number MOST 109-2221-E-008-004-MY2.

Declarations

Funding This research was supported by the Ministry of Science and Technology in Taiwan, project number MOST 109-2221-E-008-004-MY2.

Competing interests The authors declare no competing interests.

Availability of data and material All data generated or analyzed during this study are included in the manuscript.

Code Availability Not applicable.

Ethics approval Ethical standards are in place (no human participants or animals involved).

Consent to participate Not applicable.

Consent for publication All involved authors have read and consented to publish the manuscript.

Authors' contributions Moeso Andrianto constructed the research design, accomplished the analytical simulation, conducted the virtual simulation, and composed the manuscript, Yu-Ren Wu earned the funding and directed the research implementation, whereas Achmad Arifin supervised the analytical and virtual simulation. All authors worked concurrently to proofread and structure the submission.

References

[1] L. Wang, Y. He, Y. Wang, Y. Li, C. Liu, S. Wang, and Y. Wang (2020) Analytical modeling of material removal mechanism in dry whirling milling process considering geometry, kinematics and mechanics. International Journal of Mechanical Sciences 172:105419. https://doi.org/10.1016/j.ijmecsci.2020.105419

[2] S. Q. Song and D. W. Zuo (2014) Modelling and simulation of whirling process based on equivalent cutting volume. Simulation Modelling Practice and Theory 42:98–106. https://doi.org/10.1016/j.simpat.2013.12.011

[3] Y. He, L. Wang, Y. Wang, Y. Li, S. Wang, Y. Wang , C. Liu, and C. Hao (2019) An analytical model for predicting specific cutting energy in whirling milling process. Journal of Cleaner Production 240:118181. https://doi.org/10.1016/j.jclepro.2019.118181

[4] L.V. Mohan and M.S. Shunmugam (2007) Simulation of whirling process and tool profiling for machining of worms. Journal of Materials Processing Technology 185:191-197. https://doi.org/10.1016/j.jmatprotec.2006.03.115

[5] T. Matsumura, M. Serizawa, T. Ogawa, and M. Sasaki (2015) Surface dimple machining in whirling. Journal of Manufacturing Systems 37:487-493. https://doi.org/10.1016/j.jmsy.2014.07.008

[6] M. Soshi, F. Rigolone, J. Sheffield, and K. Yamazaki (2018) Development of a directly-driven thread whirling unit with advanced tool materials for mass-production of implantable medical parts. CIRP Annals - Manufacturing Technology 1:117-120. https://doi.org/10.1016/j.cirp.2018.03.016

[7] C. Liu, Y He, Y Li, Y Wang, L. Wang, S. Wang, and Y. Wang (2021) Predicting residual properties of ball screw raceway in whirling milling based on machine learning. Measurement 173:108605. https://doi.org/10.1016/j.measurement.2020.108605

[8] C. Liu, Y He, Y. Wang, Y. Li, S. Wang, L. Wang, and Y. Wang (2019) An investigation of surface topography and workpiece temperature in whirling milling machining. International Journal of Mechanical Sciences 164:105182. https://doi.org/10.1016/j.ijmecsci.2019.105182

[9] Y. Wang, C. Yin, L. Li, W. Zha, X. Pu, Y. Wang, J. Wang, and Y. He (2020) Modeling and optimization of dynamic performances of large-scale lead screws whirl milling with multi-point variable constraints. Journal of Materials Processing Technology 276:116392. https://doi.org/10.1016/j.jmatprotec.2019.116392

[10] Y. He, C. Liu, Y. Wang, Y. Li, S. Wang, L. Wang, and Y. Wang (2019) Analytical modeling of temperature distribution in lead-screw whirling milling considering the transient un-deformed chip geometry. International Journal of Mechanical Sciences 157-158: 619-632. https://doi.org/10.1016/j.ijmecsci.2019.05.008

[11] M. Serizawa, M. Suzuki, T. Matsumura (2015) Microthreading in Whirling. Journal of Micro- and Nano-Manufacturing 3: 041001-1. https://doi.org/10.1115/1.4030704

[12] H. S. Yan and H. H. Chen (1996) Geometry design of globoidal cams with generalized meshing turret-rollers. Journal of Mechanical Design 118. https://doi.org/10.1115/1.2826876

[13] D. M. Tsay, N. J. Huang, and B. J. Lin (1999) Geometric design of roller gear cam reducers. Journal of Mechanical Design 121. https://doi.org/10.1115/1.2829420

[14] P. D. Lin and M. F. Lee (1997) Applications of D-H notation in machining and on-line measurement of roller-gear cams on 5-axis machine tools. Journal of Manufacturing Science and Engineering 119. https://doi.org/10.1115/1.2831119
[15] S. L. Chen and S. F. Hong (2008) Surface generation and fabrication of roller gear cam with spherical rollers. Journal of Advance Mechanical Design, System, and Manufacturing 2:3. https://doi.org/10.1299/jamdsm.2.290
[16] H. S. Yan and H. H. Chen (1994) Geometry design and machining of roller gear cams with cylindrical rollers. Mechanism and Machine Theory 29:6. https://doi.org/10.1016/0094-114X(94)90079-5
[17] T. N. Van and P. Pokorny (2009) Modelling concave globoidal cam with indexing turret follower: A case study. International Journal of Computer Integrated Manufacturing 22:10. https://doi.org/10.1080/09511920902943655
[18] J. S. Lo, C.H. Tseng and C.B. Tsay (2001) A study on the bearing contact of roller gear cams. Comput. Methods Appl. Mech. Engrg. 190:4649-4662. https://doi.org/10.1016/S0045-7825(00)00337-6
[19] F.L. Litvin and A. Fuentes (2004) Gear Geometry and Applied Theory, 2nd ed., Cambridge University Press, Cambridge, UK. https://doi.org/10.1017/CBO9780511547126
[20] H.S. Yan and H.H. Chen (1995) Geometry design of roller gear cams with hyperboloid rollers. Mathl. Comput. Modelling 22(8):107-117. https://doi.org/10.1016/0895-7177(95)00160-4
[21] Y. Zhang, S. Ji and J. Zhao (2016) Study on the geometric characteristics of mating surfaces of globoidal cam mechanisms. Mechanism and Machine Theory 100:44–62. https://doi.org/10.1016/j.mechmachtheory.2016.01.014
[22] C. Zongyu, Z. Ce, Y. Yuhu, and W. Yuxin (2001) A study on dynamics of roller gear cam system considering clearances. Mechanism and Machine Theory 36:143-152. https://doi.org/10.1016/S0094-114X(00)00038-0
[23] M. Wan, W.H. Zhang, J.W. Dang, and Y. Yang (2010) A novel cutting force modelling method for cylindrical end mill. Applied Mathematical Modelling 34:823–836. https://doi.org/10.1016/j.apm.2009.09.012
[24] R. Whalley, A.A. Abdul-Ameer, and M. Ebrahimi (2008) Machine tool modelling and profile following performance. Applied Mathematical Modelling 32:2290–2311. https://doi.org/10.1016/j.apm.2007.07.017
[25] C. Neagu, M. Lupeanu, and A. Rennie (2013) A new design concept for milling tools of spherical surfaces obtained by kinematic generation. Applied Mathematical Modelling 37:6119–6134. https://doi.org/10.1016/j.apm.2012.12.017
[26] T. Sekine and T. Obikawa (2015) Novel path interval formulas in 5-axis flat end milling. Applied Mathematical Modelling 39:3459–3480. https://doi.org/10.1016/j.apm.2014.11.046
[27] K. Sambhav, P. Tandon, and S. G. Dhande (2011) A generic mathematical model of single point cutting tools in terms of grinding parameters. Applied Mathematical Modelling 35:5143–5164. https://doi.org/10.1016/j.apm.2011.04.017
[28] K. Jia, J. Guo , S. Zheng , and J. Hong (2019) A general mathematical model for two-parameter generating machining of involute cylindrical gears. Applied Mathematical Modelling 75:37-51. https://doi.org/10.1016/j.apm.2019.05.021
[29] Y. R. Wu and W. H. Hsu (2014) A general mathematical model for continuous generating machining of screw rotors with worm-shaped tools, Applied Mathematical Modelling 38:28–37. https://doi.org/10.1016/j.apm.2013.05.056
[30] G. Urbikaina, E. Artetxe, L. N. L. de Lacalle (2017) Numerical simulation of milling forces with barrel-shaped tools considering runout and tool inclination angles. Applied Mathematical Modelling 47:619–636. https://doi.org/10.1016/j.apm.2017.03.001
[31] S. P. Radzevich (2007) A novel method for mathematical modeling of a form-cutting-tool of the optimum design. Applied Mathematical Modelling 31:2639–2654. https://doi.org/10.1016/j.apm.2006.10.014
[32] F. Chen, S. Hu and S. Yin (2012) A novel mathematical model for grinding ball-end milling cutter with equal rake and clearance angle. International Journal of advanced Manufacturing Technology 63:109–116. https://doi.org/10.1007/s00170-011-3889-y
[33] M. R. Khan and P. Tandon (2011) Mathematical modeling for the design of a generic custom-engineered form mill. International Journal of advanced Manufacturing Technology 54:139–148. https://doi.org/10.1007/s00170-010-2936-4
[34] Z Pálmai and L Csobod (2017) The mathematical modelling of the impact of electric (Seebeck) effects on end-milling. International Journal of advanced Manufacturing Technology 88:115–126. https://doi.org/10.1007/s00170-016-8696-z
[35] X. Ming, Q. Gao, H. Yan, J. Liu and C. Liao (2017) Mathematical modeling and machining parameter optimization for the surface roughness of face gear grinding. International Journal of advanced Manufacturing Technology 90:2453–2460. https://doi.org/10.1007/s00170-016-9576-2

[36] X. Jing, B. Song, J. Xu and D. Zhang (2022) Mathematical modeling and experimental verification of surface roughness in micro-end-milling. International Journal of advanced Manufacturing Technology 120:7627–7637. https://doi.org/10.1007/s00170-022-09244-7

[37] M. Andrianto, Y. R. Wu, and A. Arifin (2022) A novel manufacturing method for double-enveloping worms using a whirl-machining process. Mechanism and Machine Theory 179: 105099. https://doi.org/10.1016/j.mechmachtheory.2022.105099